

1 **ENSO Transition, Duration and Amplitude asymmetries: Role of**
2 **the nonlinear wind stress coupling in a conceptual model**

KIT-YAN CHOI *

3 *Princeton University, Princeton, New Jersey*

GABRIEL A. VECCHI AND ANDREW T. WITTENBERG

4 *Geophysical Fluid Dynamics Laboratory and Princeton University, Princeton, New Jersey*

* *Corresponding author address:* Kit-Yan Choi, Princeton University 201 Forrestal Road, Princeton, NJ 08540.

E-mail: kityanc@princeton.edu

ABSTRACT

6 The El Niño/Southern Oscillation (ENSO) exhibits well-known asymmetries: (1) warm
7 events are stronger than cold events; (2) strong warm events are more likely to be followed
8 by cold events than vice versa; and (3) cold events are more persistent than warm events.
9 Coupled GCM simulations, however, continue to underestimate many of these observed
10 features.

11 To shed light on these asymmetries, we begin with a widely-used delayed-oscillator con-
12 ceptual model for ENSO, and modify it so that wind stress anomalies depend more strongly
13 on SSTAs during warm conditions - as is observed. We then explore the impact of this
14 nonlinearity on three dynamical regimes for ENSO: self-sustained oscillations, stochastically
15 driven oscillations, and self-sustained oscillations interrupted by stochastic forcings. In all
16 three regimes, the nonlinear air-sea coupling preferentially strengthens the feedbacks (both
17 positive and delayed negative) during the ENSO warm phase – producing El Niños that grow
18 to larger amplitude and overshoot more rapidly and consistently into the opposite phase,
19 than do the La Niñas. Finally, we apply the modified oscillator to observational records, and
20 to control simulations from two global coupled ocean-atmosphere-land-ice models (GFDL-
21 CM2.1 and GFDL-CM2.5), to elucidate the causes of their differing asymmetries.

1. Introduction

Fluctuations of the El Niño/Southern Oscillation (ENSO) involve coupled changes to the ocean and atmosphere. During the warm phase of ENSO, the prevailing easterly winds over the central Pacific weaken; these westerly wind anomalies advect warm surface water toward the east, reduce the zonal slope of the thermocline and inhibit the upwelling of cold water in the eastern Pacific, which feeds back positively on the warming of surface water in the eastern Pacific and allows small perturbations to grow. This positive feedback is also known as the Bjerknes feedback (Bjerknes 1969). To first approximation, La Niña (the cold phase) anomalies are roughly the opposite of those of El Niño (Larkin and Harrison 2002, hereafter LH2002). Theories proposed to explain the termination of El Niño (La Niña) and its transition into the opposite phase include the reflection of oceanic internal waves at the eastern and western boundaries (Suarez and Schopf 1988; Battisti and Hirst 1989, hereafter BH1989), recharge and discharge of equatorial warm water due to Sverdrup balance (Jin 1997), western Pacific wind-forced Kelvin waves (Weisberg and Wang 1997), and anomalous zonal temperature advection by oceanic currents (Picaut et al. 1997). These theories agree that oceanic adjustments result in delayed negative feedbacks that explain the turnabout between El Niño and La Niña, with simple models illustrating how these mechanisms can result in oscillatory behavior for ENSO. Although nonlinearity has been shown to impact the growth and decay of El Niño (Tziperman et al. 1997; Gebbie et al. 2007; Vecchi 2006; Vecchi and Harrison 2006), linear techniques that are widely used for studying ENSO, such as empirical orthogonal function (EOF) analysis and linear regression, tend to treat El Niño and La Niña as simple mirror images of each other.

For all the approximate symmetries of El Niño and La Niña events, considerable asymmetry does exist. Most noted in past literature is the amplitude asymmetry of ENSO, namely that El Niño tend to be stronger than La Niña (Burgers and Stephenson 1999). Several oceanic mechanisms have been proposed for this asymmetry: nonlinear dynamical heating (Jin et al. 2003; An and Jin 2004) and negative feedback due to tropical instability waves

49 which are stronger during La Niña (Wang and McPhaden 2000; Vialard et al. 2001). A
50 common element of all these proposed mechanisms is their inherent oceanic origin.

51 Other studies have drawn attention to the asymmetric atmospheric response to sea surface
52 temperature changes. Kang and Kug (2002) studied a hybrid atmosphere-ocean coupled
53 model, and suggested that the relatively weaker sea surface temperature anomalies (SSTA)
54 and shorter duration for La Niña are attributable to the westward shift of the wind stress
55 anomalies (Hoerling et al. 1997). Philip and van Oldenborgh (2009), Frauen and Dommenges
56 (2010) found that a nonlinear zonal wind response to opposite sign SST anomalies may have
57 an important influence on the SST skewness in the eastern tropical Pacific. Dommenges et al.
58 (2013) suggest that the skewness in SST is related to the asymmetries in the pattern shape
59 and the time evolution of ENSO events which can be partially attributed to the nonlinear
60 response of the zonal wind to SST anomalies. Nonlinear relationships between the seasonal
61 cycle and ENSO as well as the origins of the ENSO's phase locking to the seasonal cycle
62 were also studied (Harrison and Vecchi 1999; Galanti and Tziperman 2000; Tziperman et al.
63 1997; Galanti et al. 2002).

64 In addition to amplitude asymmetry, there are other differences in the evolution of El
65 Niño and La Niña. LH2002 characterized differences in the life cycles of the warm and
66 cold phases by examining the ENSO behavior phase-by-phase. In their appendix, LH2002
67 note that warm-to-cold transitions tend to occur within a single year, with the cold event
68 emerging the year following the warm event. In contrast, cold-to-warm transitions occur
69 over 1-3 years. Okumura and Deser (2010) also showed that there is a robust asymmetry
70 in the duration of El Niño and La Niña in observations, with La Niña persisting longer, a
71 feature also noted by Kessler (2002). Subsequently, Okumura et al. (2011) proposed that an
72 asymmetric wind response due to delayed SST forcing in the Indian Ocean acts to prolong
73 La Niña.

74 Various observational datasets of Pacific surface wind stress support the hypothesis that
75 during ENSO, the wind stress response to the SST anomalies is weaker in the cold phase

76 than in the warm phase. Figure 1 shows regression coefficients of zonal wind stress anomalies
77 onto the Niño-3.4 SSTA index (area average of SST anomalies at 5°S– 5°N, 170°W – 120°W)
78 during warm and cold conditions, for the FSU observational wind product (see Section 2).
79 The asymmetry in the sensitivity is also evident in other estimates of wind stress. Figure
80 2 shows scatter plots of the zonal wind stress anomalies averaged over a 40° longitude by
81 10° latitude region where the regression coefficients are largest versus the observed Niño-3.4
82 SSTA index, from 2 months before an event peak to 2 months after the peak. The averaging
83 area is also shifted zonally according to where the regression coefficients are the largest for a
84 particular ENSO phase. It is clear that wind stress responds more sensitively to sea surface
85 temperature anomalies during warm conditions.

86 In this study, we have explored the impact of this atmospheric nonlinearity on the sym-
87 metry of ENSO. We will parametrize this effect in a simple model, by having the air-sea
88 coupling efficiency be dependent on the ENSO polarity; and we explore how this dependence
89 can cause asymmetries in the duration, amplitude and sequencing of ENSO. In Section 2,
90 we describe the observational datasets and GCM outputs to which we apply the measures
91 described in Section 3 to identify these three aspects of asymmetry. The formulation of the
92 conceptual ENSO model used is given in Section 3. The results are presented and analyzed
93 in Section 4. Section 5 gives a summary and further discussions.

94 [Figure 1 about here.]

95 [Figure 2 about here.]

96 **2. Data sources**

97 *a. SST data*

98 There are uncertainties in past reconstructions of the tropical Pacific SST (Vecchi et al.
99 2008) and we therefore explore two SST datasets: HadISST and ERSST version 3b.

100 1) HADISST

101 The Hadley Centre sea ice and sea surface temperature dataset for 1880 – 2012 (HadISST;
102 Rayner et al. 2003) is used for computing the Niño–3.4 SSTA index. We examine the his-
103 torical record entirely as well as in segments. Monthly climatologies are computed over the
104 period of time series sampled, and the anomalies are computed by subtracting the clima-
105 tologies from the original record. The HadISST Niño–3.4 SST anomalies have increased by
106 0.2 degrees from 1880 to 2012.

107 2) ERSST v3B

108 The Extended Reconstructed Sea Surface Temperature (ERSST) Version 3b (Smith et al.
109 2008) provided by NOAA is used as another long-term SST observational record to compare
110 with HadISST. The dataset spans from 1854 to present. In the current study, the time series
111 from 1880 to 2012 is used since the strength of the signal becomes more consistent after
112 1880. This version of SST analysis uses in situ SST data and improved statistical methods.
113 Unlike the version 3, satellite data that causes a small cold bias is not used in version 3b.
114 From 1880 to 2012, ERSST Niño–3.4 SST anomalies have increased by 0.6 degree.

115 The warming trends in the HadISST and ERSST products are included in the analysis
116 presented below. The Niño–3.4 temperature anomalies are also smoothed using a running
117 5-month boxcar average before analysis. We will discuss the sensitivity of the results to
118 whether the time series is detrended or not.

119 *b. Surface wind stress estimates*

120 There are also large uncertainties in reconstructions of wind stress over the Pacific (Wit-
121 tenberg 2004), so we use multiple wind stress estimates in our analysis. Observational
122 datasets used here for the wind stress response analysis are: the COAPS third-generation
123 Florida State University objectively Gridded Pacific monthly mean in-situ flux products

124 (FSU3; Bourassa et al. 2005) from 1987 to 2004; the 40-year European Centre for Medium-
125 Range Weather Forecast (ECMWF) Reanalysis (ERA-40; Uppala et al. 2005) 6-hourly mo-
126 mentum stress product from 9/1957 to 8/2002; ECMWF Interim Reanalysis (ERA-Interim;
127 Dee and Uppala 2009) from 1979 to 2011; NASAs Modern-Era Retrospective Analysis for
128 Research and Applications (MERRA; Rienecker et al. 2011) from 1979 to 2010 and the
129 National Centers for Environmental Prediction-National Center for Atmospheric Research
130 (NCEP–NCAR) Reanalysis (NCEP1; Kalnay et al. 1996; Kistler et al. 2001) from 1948 to
131 2011.

132 *c. Coupled GCMs*

133 1) GFDL CM2.1

134 CM2.1 is a Geophysical Fluid Dynamics Laboratory (GFDL) global coupled atmosphere-
135 ocean-land-ice GCM. The detailed formulations are described by Delworth et al. (2006) (and
136 references therein). Wittenberg et al. (2006) describes the behavior of ENSO in this model.
137 The CM2.1 has taken part in the Third and Fifth Coupled Model Intercomparison Project
138 (CMIP3 and CMIP5) and the Fourth Assessment of the Intergovernmental Panel on Climate
139 Change (IPCC). In this study, we use the monthly mean output of the pre-industrial control
140 experiment integrated for 4000 years with fixed 1860 estimates of solar irradiance, land cover,
141 and atmospheric composition. The long run provides more than 300 El Niño and 300 La
142 Niña events, and thus allows statistically significant analysis of the behavior of simulated
143 ENSO. The description of the interdecadal variability of ENSO for the first 2200-years of
144 this experiment is described in Wittenberg (2009).

145 2) GFDL CM2.5

146 CM2.5 is a newer, higher resolution (atmosphere/land horizontal resolution is 0.5 degree
147 instead of 2 degree; ocean/sea ice resolution is about 0.25 degree instead of 1 degree), global

148 coupled GCM based on CM2.1. The two models are initialized and forced in a similar
149 fashion. The resolutions of the atmosphere and ocean components in CM2.5 are increased.
150 A smaller viscosity is used in CM2.5. Parametrized eddy mixing is excluded in the CM2.5
151 ocean, while it is included in CM2.1. Further details on CM2.5 and comparisons with CM2.1
152 are documented in Delworth et al. (2012). The data used in this study is based on a 260-year
153 control experiment using fixed 1990 estimates of solar irradiance, land cover and atmospheric
154 composition. 37 El Niños and 34 La Niñas are identified in this experiment.

155 3) COMPARISON OF THE SIMULATED ENSO IN CM2.5 AND CM2.1 WITH OBSERVA- 156 TIONS

157 Delworth et al. (2012) describe how the simulated ENSO in CM2.5 compares to CM2.1
158 and observations. More detailed descriptions of the CM2.1 ENSO behavior can be found in
159 Wittenberg et al. (2006). Here we summarize some of their results.

160 ENSO amplitude in CM2.5 is weaker and is closer to observations, while CM2.1 tends to
161 simulate ENSO events that are too strong. While both models have equatorial Pacific SST
162 anomalies that extend too far to the west, this bias is reduced in CM2.5.

163 Both models have problems simulating the seasonal phase locking of ENSO. The CM2.1
164 ENSO shows almost no seasonal phase locking, except that the Niño-3.4 index has a slight
165 tendency to peak between October and February and strong events tend to lock better to
166 the seasonal cycle. CM2.5 Niño-3.4 index has better phase locking compared to CM2.1, but
167 is still weaker and later than observations by about a month.

168 At interannual time scales, the spectrum of tropical Pacific SSTs in CM2.5 is too con-
169 centrated at about 2.5 years. CM2.1 shows a broader and more realistic spectrum, but is
170 stronger than the observations at interannual time scales. Accordingly, the ENSO in CM2.5
171 is noticeably more regular than CM2.1 and the observed. However, the lengths of obser-
172 vational records are short, so the spectra in this frequency band are uncertain (Wittenberg

173 2009; Vecchi and Wittenberg 2010).

174 **3. Methods**

175 *a. The conceptual ENSO model*

Following the delayed-oscillator model proposed by BH1989, which is closely related to the models studied by Suarez and Schopf (1988) and Zebiak and Cane (1987), we model ENSO as arriving from two essential drivers. First, the Bjerknes positive feedback that leads to instability; second, a delayed negative feedback that results in oscillations. We thereby use a conceptual model of ENSO based on the BH1989 model:

$$\frac{\partial T}{\partial t} = -bT + c'\tau^x(t - t_1) - d'\tau^x(t - t_2) - \epsilon T^3 \quad (1)$$

176 where T is the Niño-3.4 SST anomaly. τ^x is the wind stress anomaly at the central equatorial
177 Pacific near the date line. t_1 is the time required for wind stress response to positively
178 feedback to surface temperature T . t_2 is the time required for the negative feedback to
179 enact. t_1 is smaller than t_2 . b , c' and d' are positive scalar parameters. ϵ is non-zero when
180 the system is unstable otherwise. The current settings for t_1 and t_2 are 1 and 6 months,
181 which are roughly the time required for the first/second baroclinic Kelvin wave to propagate
182 eastward from the date line to the American coasts and the time required for Rossby waves
183 to propagate westward, and reflect back as Kelvin waves to the eastern Pacific (Harrison and
184 Giese 1988; Harrison and Vecchi 1999). The qualitative conclusion is unchanged if different
185 values of t_1 and t_2 are used as long as $t_2 > t_1$. If $t_1 = 0$, one recovers the BH1989 formulation.

186 The first term on the right-hand side of Eq(1) is a qualitative representation of local
187 dampings of T due to air-sea fluxes, the mean zonal advection of the anomalous zonal
188 temperature gradient and the mean vertical advection of the anomalous temperature gradient
189 that depends on T . Guided by BH1989 and regression analysis on these processes at the
190 eastern Pacific, the value of b is kept fixed at 0.24/mon throughout the entire study.

191 The second and the third terms are the positive and the delayed-negative feedbacks. Each
 192 of these two terms incorporates the anomalous zonal advection of the mean zonal tempera-
 193 ture gradient, (part of the) mean vertical advection of the anomalous vertical temperature
 194 gradient and the anomalous vertical advection of the mean vertical temperature gradient.

By construction, Eq(1) gives a symmetric oscillator in which warm and cold maxima have
 equal persistence, frequencies and amplitudes. To break the symmetry, we write $\tau^x = \tau^x(T)$
 such that the wind stress anomalies respond more sensitively to warm SST anomalies than
 to cold SST anomalies. For simplicity, we write τ^x as a piecewise linear function of T , i.e.:

$$\tau^x = \gamma (T + r |T|) \quad (2)$$

195 where γ (unit: Pa/K) and r (nondimensional) are both scalar parameters. For r positive
 196 and less than 1, wind stress anomalies are stronger for the same degree of positive T than
 197 negative T .

From the regression analysis of wind stress response to SST anomalies (Fig 1), we can
 estimate r from the difference in the regression slopes:

$$r = \frac{s_w - s_c}{s_w + s_c} \quad (3)$$

198 where s_w , s_c are the slopes for warm and cold events respectively.

199 Table 1 summarizes the value of r estimated from different datasets. Most datasets
 200 produce an r of about 20% with the exception of NCEP-1. This agrees with the suggestion
 201 made by (Wittenberg 2004) that FSU is recommended over NCEP-1 for extended studies of
 202 ENSO since the former dataset agrees better with other observations and updated analysis.
 203 Why the NCEP-1 does not show the nonlinear relationship between the zonal wind stress
 204 and SST during ENSO, as is seen in other datasets, is unclear.

205 [Table 1 about here.]

206 In addition to the asymmetry in the intensity of the wind response, it is likely that the
 207 zonal shift in the wind stress patterns (Fig 1) between El Niño and La Niña may also be

208 an important feature of ENSO (Kang and Kug 2002). However, we forgo investigation of
209 pattern-change effects in the present study, in order to focus more intensely on the effects of
210 the wind stress strength anomaly.

211 Further regression analysis of the wind stress response shows that CM2.1 has a large
212 estimated value of r about 46%, much higher than the observed. Conversely, CM2.5 has a
213 smaller value of r (= 15%).

214 As in BH1989, there are two key regions in the parameter space, one being a stable
215 region in which the oscillator is damped, another being an unstable region in which small
216 perturbations in the oscillator grow to infinity. The unstable regime can be further divided
217 into the an oscillatory and a non-oscillatory regime. To sustain an oscillation for the stable
218 region, a stochastic wind forcing is superimposed on τ^x . The stochastic forcing has an
219 amplitude that is normally distributed with mean zero and a standard deviation σ (unit:
220 Pa), and has a decorrelation time of 0.2 months. For the unstable region, no stochastic
221 forcing is added, but ϵ in Eq(1) would be non-zero to stabilize the oscillation (BH1989). The
222 stability characteristics across the parameter space are shown in Figure 3. A few examples
223 of the parameter regimes 1 and 2 are shown in Figure 4. Region 1 is the linearly stable,
224 damped region with $\epsilon = 0$. Region 2 is the linearly unstable region but is nonlinearly stable
225 using $\epsilon > 0$. Region 3 is unstable when $\epsilon = 0$; with $\epsilon > 0$, the oscillation dies quickly and
226 converges to a constant non-zero value, which is far from the observed behavior. Regime 3
227 is not considered in the rest of this study.

228 [Figure 3 about here.]

229 [Figure 4 about here.]

With stochastic forcing, Eq. (2) becomes

$$\tau^x = \gamma (T + r |T|) + N(t) \quad (4)$$

where N is Gaussian white noise with zero mean and standard deviation σ . Eq(1) can be

written more compactly as

$$\frac{\partial T}{\partial t} = -bT + c[T(t - t_1) + r|T(t - t_1)|] - d[T(t - t_2) + r|T(t - t_2)|] + c'N(t - t_1) - d'N(t - t_2) - \epsilon T^3 \quad (5)$$

230 where $c = \gamma c'$ and $d = \gamma d'$ now have units of 1/month. σ is non-zero only in region 1
 231 unless otherwise specified. ϵ ($\epsilon > 0$) is non-zero only in region 2 and 3. The values of σ and
 232 ϵ are tuned so that the simulated T has a standard deviation of roughly 0.8K, in order to be
 233 compared with the observations. The values of σ and ϵ do not alter qualitative conclusions
 234 of this paper regarding the asymmetry of the simulated ENSO.

235 Since the stochastic forcing is independent of T and the additional damping is an odd
 236 function of T , neither of these two functions should introduce asymmetries. Any asymmetry
 237 in this model will be attributable entirely to τ^x as a piecewise function of T . This permits
 238 a focused look at the impacts of this particular nonlinearity, as a foundation for future
 239 inclusion of other nonlinearities. In this paper we present figures using $r = 0\%$ and $r = 60\%$
 240 for apparent and clear comparisons; we have also explored other intermediate values of r
 241 and showed some results using $r = 20\%$ and $r = 40\%$.

242 *b. Definitions of ENSO phases and asymmetry*

243 To compare the conceptual model results with the observations and GCMs, consistent
 244 definitions of ENSO events, peaks and durations are needed. Despite the richness of the
 245 ENSO phenomenon (e.g. LH2002; Wolter and Timlin 2011), we use the sea surface temper-
 246 ature anomaly in the central/eastern Pacific Ocean Niño-3.4 box as a proxy to illustrate the
 247 asymmetries of ENSO in observations and GCMs. To consistently compare the conceptual
 248 model results with the observations and GCMs, the same recipe is applied to the time series
 249 T simulated by the conceptual model.

250 El Niño (La Niña) is defined such that the 5-month running mean of the Niño-3.4 index
 251 exceeds (is below) its 90-th (10-th) percentile of the time series, for at least 3 consecutive

252 months. Other percentiles (e.g. 85-th/15-th) have been explored, and the fundamental
253 results remain roughly the same. The years of warm and cold events in the observational
254 datasets are summarized in Figure 5. Figure 6 illustrates the criteria for defining events,
255 terminations and durations, as will be described below.

256 [Figure 5 about here.]

257 The termination time of events is calculated by the time lapse from the event peak to
258 the time when the Niño-3.4 index first comes within 25% of the standard deviation from the
259 time mean. If an event persists and reintensifies into another event of the same sign such
260 that both events terminate at the same time, the preceding event is not considered in the
261 duration analysis to avoid double counting.

262 The asymmetry in sequencing is examined by calculating the sample conditional proba-
263 bilities of different types of transitions. This analysis is more uncertain for the observations
264 largely due to the ambiguity of how one identifies a transition type and the inadequate num-
265 ber of events. To be consistent across observational datasets and GCM outputs, we adopt
266 the following procedures when calculating the event transition probability:

- 267 i. Identify the El Niño and La Niña events using the 90-th and 10-th percentiles and
268 persistence criteria
- 269 ii. For each warm or cold event, for example, a warm event:
 - 270 - identify when the event terminates
 - 271 - if the next event is a cold (warm) event and occurs within 12 months after the
272 termination, this is identified as a warm-to-cold (warm-to-warm) transition

Following these procedures, transition probabilities are calculated such that

$$P_{\text{warm-to-warm}} + P_{\text{warm-to-cold}} + P_{\text{warm-to-else}} = 1$$

$$P_{\text{cold-to-cold}} + P_{\text{cold-to-warm}} + P_{\text{cold-to-else}} = 1$$

273 [Figure 6 about here.]

274 4. Results

275 a. *Observations and GCM*

276 In the observational record and the models, more warm events terminate within a year
277 after peaks than cold events do. Figure 7 shows the cumulative distribution of termination
278 times for warm and cold events for the observational datasets and global climate models’
279 control run outputs. This result is consistent with LH2002 and Okumura and Deser (2010).
280 If the Niño–3.4 SSTA time series is detrended, cold events appear to last much longer, i.e.
281 the asymmetry in duration is amplified upon detrending.

282 Following the procedures described in Section 3, conditional probabilities for different
283 transition types are calculated and shown in Figure 8. From the observations, there is a
284 higher likelihood to have warm events be followed by cold events than vice versa. Cold-
285 to-cold transitions are also more frequent than warm-to-warm transitions. This qualitative
286 conclusion holds even when a linear trend is removed from the Niño–3.4 SST index. The
287 numbers of observed warm and cold events are so small that the statistical significance
288 varies with the choice of Niño–3.4 SSTA thresholds as well as whether or not a linear trend
289 is removed. In contrast, the control runs of CM2.1 and CM2.5 offer larger samples of El Niño
290 and La Niña. The asymmetry in sequencing is consistently very strong in the CM2.1 control
291 run, with warm-to-cold transitions much more likely than cold-to-warm transitions. CM2.5
292 shows an asymmetry in favor of warm-to-cold transitions that is weaker than in CM2.1 but
293 is similar to the observations. Cold-to-cold transitions are very rare in both models.

294 Skewness is a useful measure to represent the amplitude asymmetry, as is summarized
295 in Table 2. The Niño–3.4 SSTA index in the observations and CM2.1 have very consistent
296 positive skewness, indicating stronger warm anomalies. CM2.5, however, with a more regular
297 ENSO, shows a small negative skewness with Niño–3.4 index and a small positive skewness
298 with Niño-3 index.

299 [Table 2 about here.]

300

[Figure 7 about here.]

301

[Figure 8 about here.]

302 *b. The conceptual ENSO model with $r > 0$*

303

304

305

306

307

We have analyzed results using different values of r . Table 2 summarizes the asymmetries that the conceptual model is capable of at $r = 20\%$ and $r = 40\%$. Since more points in the c - d parameter space (i.e. fixing b) would show significant asymmetries with larger values of r . Figures in this section present results using $r = 60\%$ for illustrative purposes. All the qualitative results hold true for other positive values of r .

308

1) ASYMMETRY IN AMPLITUDE

309

310

311

312

313

314

315

316

317

Figure 9 shows the skewness across the c - d parameter space with $r = 60\%$. (The magnitude of the skewness increases with increasing values of r .) The skewness can be positive or negative depending on the relative strength of the positive and negative feedback, i.e. the ratio of c and d . If c/d is large, extreme SST anomalies depend more on the instability brought by the positive feedback, i.e. had the damping term been smaller, the system would be non-oscillatory and grow to infinity due to the strong positive feedback. In this case, positive feedback is enhanced with a larger coupling efficiency during warm events. Therefore, warm events are able to grow to larger amplitudes while cold events become relatively weak, resulting in a positive skewness.

318

319

320

321

322

323

Instead, if d/c is large, extreme SST anomalies depend more on the strong overshooting of the preceding events of the opposite sign, i.e. the system would be oscillatory unstable if the damping term was not strong enough. Therefore cold events can grow to larger amplitudes due to the stronger delayed cooling of the preceding warm events, while warm event peaks cannot grow as much since the delayed warming due to the preceding cold events is diminished. In short, if the coupling efficiency is larger during warm events, skewness be-

324 comes positive in the parameter region where positive feedback strength is large, or negative
325 where negative feedback strength is large. Notice that the cutoff does not lie along $c = d$
326 because b is non-zero.

327 [Figure 9 about here.]

328 2) ASYMMETRY IN DURATION

329 [Figure 10 about here.]

330 [Figure 11 about here.]

331 As r increases, cold events terminate at a later time than warm events do. This difference
332 in termination times resembles the behavior found in the observations and GCMs. Figure
333 10 shows how the distributions of event termination time change with the value of r . The
334 effect of $r > 0$ on the termination time across the parameter space is shown in Figure 11.

335 Since the delayed negative feedback is strengthened for warm events, warm events tend
336 to terminate faster than cold events do. In addition, as a cold event decays more slowly, the
337 temperature anomaly that precedes the eventual turnaround of the cold event is not as large
338 as it would have been had the event decayed more rapidly. Therefore, the slower termination
339 of cold events weakens the delayed warming and makes the termination even slower.

340 In addition, part of the longer termination time for cold events can be explained by the
341 fact that the time mean state of the system is warmer than the equilibrium state when the
342 temperature anomaly is strongly positively skewed. Taking the warmer time mean state as
343 the reference neutral state, as is done with the observational datasets, inevitably increases
344 the termination time of cold events. Nevertheless, following the contour of zero skewness in
345 Figure 9, it is clear in Figure 11 that cold events tend to last longer than warm events in
346 the conceptual model even when there is little amplitude asymmetry.

347 If stochastic forcing is also added to self-sustained oscillations in region 2 (Figure 12),
348 the spread of the termination time distribution for cold events increases more than that

349 for warm events. When the stochastic forcing intensity is moderate, high percentiles (e.g.
350 95-th) of the cold event termination time extend more to longer durations than those of the
351 warm events do. As stochastic forcing continues to amplify, the entire distribution of the
352 termination time moves to shorter time scales because the signal begins to be dominated by
353 stochastic forcing which has higher frequencies than the ENSO. This result clearly illustrates
354 the susceptibility of cold events to external forcing.

355 [Figure 12 about here.]

356 3) ASYMMETRY IN SEQUENCING

357 The conceptual model also shows a higher tendency for warm-to-cold transitions than
358 cold-to-warm transitions with $r > 0$. As shown in Figure 13, the probability of warm-to-cold
359 transitions minus that of cold-to-warm transitions are positive everywhere in the stable and
360 stochastically driven region (region 1). In the region 2, the oscillation is self-sustained and is
361 very regular. The positive difference in the transition probabilities in region 2, as shown in
362 Figure 13, is due to the fact that some of the warm events peak later than 12 months after
363 the preceding cold event termination and do not fulfill the transition criterion (see Section
364 3).

365 If stochastic forcing is added to the region 2, the probabilities of warm-to-warm and
366 cold-to-cold transitions increase, and the latter increases more than the former, albeit to a
367 slight extent (Figure 14).

368 With the delayed negative feedback being stronger following warm events, and weaker
369 following cold events, warm events are more likely to be plunge into cold events than vice
370 versa – since the cooling following warm events is strong enough to overshoot, and is more
371 resilient to disruptive stochastic forcing. In contrast, the weakened delayed warming during
372 the termination of a cold event lowers the probability of a cold-to-warm transition. This
373 explains why a stable, stochastically driven parameter region is necessary for the asymmetry

374 in sequencing to be revealed in this conceptual model.

375 [Figure 13 about here.]

376 [Figure 14 about here.]

377 **5. Summary and discussion**

378 The asymmetries of ENSO were examined using observational records, coupled climate
379 models and a simplified dynamical framework. Three asymmetries between El Niño and La
380 Niña are identified in models and observations: duration, sequencing and amplitude. The
381 duration asymmetry is the tendency of cold events to last longer than warm events do. The
382 amplitude asymmetry involves warm events tending to be stronger. The sequencing asym-
383 metry involves the tendency of warm events to be followed by cold events more readily than
384 vice versa. The central equatorial Pacific wind stress anomalies also exhibit an asymmetric
385 response to sea surface temperature anomalies in models and observations. Using the well-
386 known delayed-oscillator conceptual model, we parameterize the impact of the zonal wind
387 stress asymmetric response, and we demonstrate that this can lead to the above-mentioned
388 asymmetries in a consistent way. The duration asymmetry is a pervasive across the param-
389 eter space we have explored. The sequencing asymmetry can be obtained only if there is
390 stochastic external forcing. The amplitude asymmetry has the same sign as that observed
391 when the positive feedback is strong compared to the delayed negative feedback.

392 The asymmetries due to the additional nonlinearity to the ENSO conceptual model can
393 be understood as follows: warm events are able to grow into larger amplitudes with the
394 strengthened positive feedback. When they decay, the strengthened delayed negative feed-
395 back causes warm events to terminate faster and increases the chance of a following cold
396 event. The initial growth of the cold events comes from the preceding warm event but the
397 cooling subsides soon after onset. If the overshooting is not too strong, the weakened positive

398 feedback of cold events causes the cold events to mature at weaker amplitudes. When cold
399 events terminate, the delayed negative feedback is weaker. The slower neutralization and
400 the warmer long-term mean state are responsible for the longer durations of the cold events.
401 Cold events are also more prone to be disrupted by external forcing and are less likely to be
402 followed by a warm event. As a result, when there is a warm event, the predictability of a
403 following cold event is higher. What follows a cold event is more uncertain. This result is
404 consistent with Dommenges et al. (2013) that El Niños are mostly triggered by wind, less
405 predictable, while La Niña are more predictable.

406 The conceptual model simplifies the system into a few feedback terms and provides a
407 potential guide for investigations when a climate model simulates ENSO asymmetries that
408 are too strong or too weak. Figure 15 shows the parameter space regions where the conceptual
409 model resembles the asymmetry statistics of the observations, CM2.1 and CM2.5. Table 2
410 summarizes the best solutions and the corresponding asymmetries. We may conclude that
411 the best solutions for the observations and CM2.1 are very close to each other. The fact that
412 CM2.1 shows a stronger ENSO asymmetry may be explained by the larger r diagnosed for
413 CM2.1. The negative skewness in CM2.5, on the contrary, can be explained by the stronger
414 delayed negative feedback parameter relative to that of the positive feedback. We speculate
415 that the meridional extent of the wind stress anomaly may be the cause. Capotondi et al.
416 (2006) show that the CMIP3 coupled GCMs exhibited a pervasive bias in which their patterns
417 of wind stress anomalies were too far west and too narrow meridionally. They argued that by
418 amplifying the delayed negative feedback, this shortened the simulated ENSO period. The
419 conceptual model suggests that in the presence of asymmetric coupling ($r > 0$), the models'
420 narrow and westward-shifted wind stress response patterns could also help explain their
421 tendency toward overly-symmetric ENSO evolution. CM2.5, for example, has a particularly
422 narrow wind stress anomaly pattern, a strong diagnosed delayed negative feedback, and
423 highly symmetric ENSO behavior.

424 [Figure 15 about here.]

425 In the conceptual model, the difference in the wind stress response during warm and
426 cold conditions also leads to a time mean state that is warmer than the equilibrium state.
427 Since the equilibrium state of nature is unknown, computing anomalies from the climatology
428 has been a conventional approach in analyzing ENSO strength and duration in observations
429 and models. The time mean state, however, cannot be acquired a priori. Therefore, for
430 applications in which the mean climate state is a necessary reference for analysis (e.g. in
431 defining the onset or termination of an event), we suggest that the impact of changes in
432 variability on the mean state be considered.

433 We also note that the seasonal cycle is not formally included in the current conceptual
434 model. However, the nonlinear wind stress response to SST anomaly is diagnosed from
435 observations and coupled climate models control experiments in which the seasonal cycle is
436 included. Therefore the current results have not excluded, entirely, the contributions of the
437 seasonal cycle on the asymmetry of ENSO.

438 The coupling efficiency dependence on the polarity of ENSO could have several causes.
439 For example, observations indicate that Westerly Wind Burst (WWB) occurrence depends
440 on the state of ENSO (Harrison and Vecchi 1997; Vecchi and Harrison 2000). The state
441 dependence of WWBs, their skewness, and their more frequent/strong occurrence at the
442 onset of warm events, would potentially be one of the processes that leads to a positive r ,
443 for example, through the low frequency component of the WWBs. GCM experiments also
444 indicate that the frequency and intensity of WWB can be promoted during El Niño due
445 to shifted location of the warmest water (Lengaigne et al. 2003). Eisenman et al. (2005)
446 suggest that this state dependence may be equivalent to an increase in the air-sea coupling
447 strength during El Niño events and Gebbie et al. (2007) show that adding a state-dependent
448 WWB parameterization to a hybrid coupled GCM increases the instability, irregularity, and
449 asymmetry of its ENSO simulation.

450 The observational data for the wind stress responses suggests $r = 20\%$ for the concep-
451 tual model. While the model at $r = 20\%$ is capable of producing realistic asymmetries

452 in amplitude and transition probability, the duration asymmetry is weaker than observed.
453 This suggests that other sources of nonlinearities, such as nonlinear dynamical heating, the
454 nonlinear relationship between the eastern Pacific thermocline depth and the SST, and the
455 nonlinear rectification of tropical instability waves, are also important in the understanding
456 of the asymmetries.

457 The current study raises a number of questions: why is the wind stress response sensitivity
458 stronger during warm events? Nonlinearities in atmospheric convections are a likely source.
459 How important are atmospheric nonlinearities compared to oceanic nonlinearities? What are
460 the roles of seasonality, ocean adjustment times and the spatio-temporal patterns of wind
461 stress coupling in the conceptual framework described here? How will future climate changes
462 affect ENSO asymmetries? We are interested in answering these questions in the future.

463 *Acknowledgments.*

464 We are indebted to Xiaosong Yang and Isaac Held for providing comments and sugges-
465 tions. This report was prepared by KC under Award NA08OAR4320752 from the National
466 Oceanic and Atmospheric Administration, U.S. Department of Commerce. The statements,
467 findings, conclusions, and recommendations are those of the author(s) and do not necessar-
468 ily reflect the views of the National Oceanic and Atmospheric Administration or the U.S.
469 Department of Commerce.

REFERENCES

- 472 An, S.-I. and F.-F. Jin, 2004: Nonlinearity and Asymmetry of ENSO. *Journal of Climate*,
473 **17 (12)**, 2399–2412.
- 474 Battisti, D. S. and A. C. Hirst, 1989: Interannual Variability in a Tropical Atmosphere–
475 Ocean Model: Influence of the Basic State, Ocean Geometry and Nonlinearity. *Journal of*
476 *the Atmospheric Sciences*, **46 (12)**, 1687–1712.
- 477 Bjerknes, J., 1969: Atmospheric Teleconnections From the Equatorial Pacific. *Monthly*
478 *Weather Review*, **97 (3)**, 163–172.
- 479 Bourassa, M. A., R. Romero, S. R. Smith, and J. J. OBrien, 2005: A New FSU Winds
480 Climatology. *Journal of Climate*, **18 (17)**, 3686–3698.
- 481 Burgers, G. and D. B. Stephenson, 1999: The normality of El Niño. *Geophysical Research*
482 *Letters*, **26 (8)**, PP. 1027–1030.
- 483 Capotondi, A., A. Wittenberg, and S. Masina, 2006: Spatial and temporal structure of trop-
484 ical pacific interannual variability in 20th century coupled simulations. *Ocean Modelling*,
485 **15 (34)**, 274–298.
- 486 Dee, D. P. and S. Uppala, 2009: Variational bias correction of satellite radiance data in the
487 ERA-Interim reanalysis. *Quarterly Journal of the Royal Meteorological Society*, **135 (644)**,
488 18301841.
- 489 Delworth, T. L., et al., 2006: GFDL’s CM2 Global Coupled Climate Models. Part I: Formu-
490 lation and Simulation Characteristics. *Journal of Climate*, **19 (5)**, 643–674.
- 491 Delworth, T. L., et al., 2012: Simulated Climate and Climate Change in the GFDL CM2.5
492 High-Resolution Coupled Climate Model. *Journal of Climate*, **25 (8)**, 2755–2781.

493 Dommenget, D., T. Bayr, and C. Frauen, 2013: Analysis of the non-linearity in the pattern
494 and time evolution of el niño southern oscillation. *Climate Dynamics*, 1–23.

495 Eisenman, I., L. Yu, and E. Tziperman, 2005: Westerly Wind Bursts: ENSOs Tail Rather
496 than the Dog? *Journal of Climate*, **18 (24)**, 5224–5238.

497 Frauen, C. and D. Dommenget, 2010: El niño and la niña amplitude asymmetry caused by
498 atmospheric feedbacks. *Geophysical Research Letters*, **37 (18)**.

499 Galanti, E. and E. Tziperman, 2000: ENSOs Phase Locking to the Seasonal Cycle in the Fast-
500 SST, fast-wave, and mixed-mode regimes. *Journal of the Atmospheric Sciences*, **57 (17)**,
501 2936–2950.

502 Galanti, E., E. Tziperman, M. Harrison, A. Rosati, R. Giering, and Z. Sirkes, 2002: The
503 Equatorial Thermocline Outcropping A Seasonal Control on the Tropical Pacific Ocean At-
504 mosphere Instability Strength. *Journal of Climate*, **15 (19)**, 2721–2739.

505 Gebbie, G., I. Eisenman, A. Wittenberg, and E. Tziperman, 2007: Modulation of westerly
506 wind bursts by sea surface temperature: A semistochastic feedback for ENSO. *Journal of*
507 *the Atmospheric Sciences*, **64 (9)**, 3281–3295.

508 Harrison, D. E. and B. S. Giese, 1988: Remote westerly wind forcing of the eastern equatorial
509 pacific; some model results. *Geophysical Research Letters*, **15 (8)**, 804807.

510 Harrison, D. E. and G. A. Vecchi, 1997: Westerly Wind Events in the Tropical Pacific,
511 198695*. *Journal of Climate*, **10 (12)**, 3131–3156.

512 Harrison, D. E. and G. A. Vecchi, 1999: On the termination of el niño. *Geophysical Research*
513 *Letters*, **26 (11)**, 15931596.

514 Hoerling, M. P., A. Kumar, and M. Zhong, 1997: El Niño, La Niña, and the Nonlinearity of
515 Their Teleconnections. *Journal of Climate*, **10 (8)**, 1769–1786.

- 516 Jin, F.-F., 1997: An Equatorial Ocean Recharge Paradigm for ENSO. Part I: Conceptual
517 Model. *Journal of the Atmospheric Sciences*, **54** (7), 811–829.
- 518 Jin, F.-F., S.-I. An, A. Timmermann, and J. Zhao, 2003: Strong El Niño events and nonlinear
519 dynamical heating. *Geophysical Research Letters*, **30**, 4 PP.
- 520 Kalnay, E., et al., 1996: The NCEP/NCAR 40-Year Reanalysis Project. *Bulletin of the*
521 *American Meteorological Society*, **77** (3), 437–471.
- 522 Kang, I.-S. and J.-S. Kug, 2002: El Niño and La Niña sea surface temperature anoma-
523 lies: Asymmetry characteristics associated with their wind stress anomalies. *Journal of*
524 *Geophysical Research*, **107**, 10 PP.
- 525 Kessler, W. S., 2002: Is ENSO a cycle or a series of events? *Geophysical Research Letters*,
526 **29**, 4 PP.
- 527 Kistler, R., et al., 2001: The NCEP/NCAR 50Year Reanalysis: Monthly Means CDROM and
528 Documentation. *Bulletin of the American Meteorological Society*, **82** (2), 247–267.
- 529 Larkin, N. K. and D. E. Harrison, 2002: ENSO Warm (El Niño) and Cold (La Niña) Event
530 Life Cycles: Ocean Surface Anomaly Patterns, Their Symmetries, Asymmetries, and Im-
531 plications. *Journal of Climate*, **15** (10), 1118–1140.
- 532 Lengaigne, M., J.-P. Boulanger, C. Menkes, G. Madec, P. Delecluse, E. Guilyardi, and
533 J. Slingo, 2003: The March 1997 Westerly Wind Event and the Onset of the 1997/98 El
534 Niño: Understanding the Role of the Atmospheric Response. *Journal of Climate*, **16** (20),
535 3330–3343.
- 536 Okumura, Y. M. and C. Deser, 2010: Asymmetry in the Duration of El Niño and La Niña.
537 *Journal of Climate*, **23** (21), 5826–5843.
- 538 Okumura, Y. M., M. Ohba, C. Deser, and H. Ueda, 2011: A Proposed Mechanism for the
539 Asymmetric Duration of El Niño and La Niña. *Journal of Climate*, **24** (15), 3822–3829.

540 Philip, S. and G. J. van Oldenborgh, 2009: Significant atmospheric nonlinearities in the
541 ENSO cycle. *Journal of Climate*, **22** (14), 4014–4028.

542 Picaut, J., F. Masia, and Y. d. Penhoat, 1997: An Advective-Reflective Conceptual Model
543 for the Oscillatory Nature of the ENSO. *Science*, **277** (5326), 663–666.

544 Rayner, N. A., D. E. Parker, E. B. Horton, C. K. Folland, L. V. Alexander, D. P. Rowell,
545 E. C. Kent, and A. Kaplan, 2003: Global analyses of sea surface temperature, sea ice, and
546 night marine air temperature since the late nineteenth century. *Journal of Geophysical*
547 *Research*, **108** (D14), 4407.

548 Rienecker, M. M., et al., 2011: MERRA: NASAs Modern-Era Retrospective Analysis for
549 Research and Applications. *Journal of Climate*, **24** (14), 3624–3648.

550 Smith, T. M., R. W. Reynolds, T. C. Peterson, and J. Lawrimore, 2008: Improvements to
551 NOAAs Historical Merged LandOcean Surface Temperature Analysis (18802006). *Journal*
552 *of Climate*, **21** (10), 2283–2296.

553 Suarez, M. J. and P. S. Schopf, 1988: A Delayed Action Oscillator for ENSO. *Journal of the*
554 *Atmospheric Sciences*, **45** (21), 3283–3287.

555 Tziperman, E., S. E. Zebiak, and M. A. Cane, 1997: Mechanisms of seasonal–ENSO inter-
556 action. *Journal of the Atmospheric Sciences*, **54** (1), 61.

557 Uppala, S. M., et al., 2005: The ERA-40 re-analysis. *Quarterly Journal of the Royal Meteor-*
558 *ological Society*, **131** (612), 29613012.

559 Vecchi, G. A., 2006: The Termination of the 199798 El Niño. Part II: Mechanisms of Atmo-
560 spheric Change. *Journal of Climate*, **19** (12), 2647–2664.

561 Vecchi, G. A., A. Clement, and B. J. Soden, 2008: Examining the Tropical Pacific’s Response
562 to Global Warming. *Eos, Transactions American Geophysical Union*, **89** (9), 81.

563 Vecchi, G. A. and D. E. Harrison, 2000: Tropical Pacific Sea Surface Temperature Anomalies,
564 El Niño, and Equatorial Westerly Wind Events. *Journal of Climate*, **13 (11)**, 1814–1830.

565 Vecchi, G. A. and D. E. Harrison, 2006: The Termination of the 1997–98 El Niño. Part I:
566 Mechanisms of Oceanic Change*. *Journal of Climate*, **19 (12)**, 2633–2646.

567 Vecchi, G. A. and A. T. Wittenberg, 2010: El Niño and our future climate: where do we
568 stand? *Wiley Interdisciplinary Reviews: Climate Change*, 1757–778.

569 Vialard, J., C. Menkes, J.-P. Boulanger, P. Delecluse, E. Guilyardi, M. J. McPhaden, and
570 G. Madec, 2001: A Model Study of Oceanic Mechanisms Affecting Equatorial Pacific
571 Sea Surface Temperature during the 1997/98 El Niño. *Journal of Physical Oceanography*,
572 **31 (7)**, 1649–1675.

573 Wang, W. and M. J. McPhaden, 2000: The Surface-Layer Heat Balance in the Equatorial
574 Pacific Ocean. Part II: Interannual Variability. *Journal of Physical Oceanography*, **30 (11)**,
575 2989–3008.

576 Weisberg, R. H. and C. Wang, 1997: A Western Pacific Oscillator Paradigm for the El
577 Niño-Southern Oscillation. *Geophysical Research Letters*, **24 (7)**, 779–782.

578 Wittenberg, A. T., 2004: Extended Wind Stress Analyses for ENSO. *Journal of Climate*,
579 **17 (13)**, 2526–2540.

580 Wittenberg, A. T., 2009: Are historical records sufficient to constrain ENSO simulations?
581 *Geophysical Research Letters*, **36**, 5 PP.

582 Wittenberg, A. T., A. Rosati, N.-C. Lau, and J. J. Ploshay, 2006: GFDL’s CM2 Global
583 Coupled Climate Models. Part III: Tropical Pacific Climate and ENSO. *Journal of Climate*,
584 **19 (5)**, 698–722.

- 585 Wolter, K. and M. S. Timlin, 2011: El niño/southern oscillation behaviour since 1871 as
586 diagnosed in an extended multivariate enso index (MEI.ext). *International Journal of*
587 *Climatology*, **31 (7)**, 10741087.
- 588 Zebiak, S. E. and M. A. Cane, 1987: A Model El Niño–Southern Oscillation. *Monthly*
589 *Weather Review*, **115 (10)**, 2262–2278.

590 List of Figures

- 591 1 Regression coefficient of FSU zonal wind stress anomalies onto the HadISST
592 Niño-3.4 index, for Niño-3.4 greater than 0.5K (top) and less than -0.5K
593 (bottom). Regions with confidence level exceeding 60% are hatched. 30
- 594 2 Regression coefficient of the area averaged zonal wind stress anomalies onto
595 the Niño-3.4 index, for Niño-3.4 greater than 0.5K (top) or less than -0.5K
596 (bottom). The HadISST Niño-3.4 index is used for the FSU and ERA-40
597 regression analysis. Reanalysis wind stress anomalies are regressed onto the
598 reanalysis Niño-3.4 indices, for MERRA and NCEP-1 respectively. Model
599 wind stress anomalies are regressed onto the model Niño-3.4 index. Area
600 averages of the wind stress are computed within the 40-degree longitude
601 box spanning from 5°S to 5°N where the regression coefficient is the largest
602 across the equatorial Pacific domain. For warm events, wind stress anomalies
603 are averaged within a box sits at 177W-137W (FSU), 176E-144W (ERA-
604 40), 176W-136W (NCEP-R1), 179W-139W (MERRA), 167E-153W (CM2.1),
605 170E-150W (CM2.5). For cold events, the box sits at 171E-149W (FSU),
606 153E-167W (ERA-40), 160E-160W (NCEP-R1), 167E-153W (MERRA), 140E-
607 180E (CM2.1), 140E-180E (CM2.5). 31
- 608 3 Stability characteristics of the conceptual model in the c - d parameter space,
609 with $b = 0.24/\text{mon}$ and $r = 0$ (left), $r = 20\%$ (middle), $r = 60\%$ (right),
610 Region 1: the system is linearly stable and sustained by normally distributed
611 stochastic forcing ($\sigma > 0$, $\epsilon = 0$). Region 2: the system is linearly unstable
612 but is limited by additional damping ($\epsilon > 0$); there is no stochastic forcing
613 ($\sigma = 0$). Region 3: unstable, non-oscillatory and is not considered in the
614 current study. 32

615	4	Sample time series of temperature anomalies. Locations in the parameter space are shown in Figure 11. (a) is an example of self-sustained oscillations free of stochastic forcings. (b) and (c) are examples of stochastically driven oscillations in a stable system.	33
616			
617			
618			
619	5	Winter years of warm and cold events identified using the percentiles criteria on HadISST (solid line) and ERSSTv3b (dashed line) datasets. Numbers above (below) the time series indicate the years when warm (cold) events peak.	34
620			
621			
622	6	A sample SST anomaly time series, filtered by 5-month running mean, illustrates how terminations, durations and transitions are defined. The segment is simulated using the conceptual model with $b = 0.24/\text{mon}$, $c = 0.49/\text{mon}$, $d = 0.26/\text{mon}$, $r = 0.6$, $\epsilon = 0.07\text{K}^{-2}\text{mon}^{-1}$ and $\sigma = 0.08\gamma \times 7\text{K} \approx 0.01\text{Nm}^{-2}$ if $\gamma = 0.02\text{Nm}^{-2}/\text{K}$. Filled circles indicate event peaks that are followed by an event of the opposite sign. Crosses indicate event peaks that are not followed by an event, under the criteria described in Section 3.	35
623			
624			
625			
626			
627			
628			
629	7	Empirical cumulative distribution of event termination time using HadISST, ERSST, CM2.1, and CM2.5. The thick lines represent results using the entire time series. For the conceptual models, thin lines represent the standard deviation among 100-year samples.	36
630			
631			
632			
633	8	Conditional Probability of transitions for warm and cold events using Niño-3.4 index	37
634			
635	9	Skewness of the simulated SST anomalies for the conceptual model with $r = 60\%$	38
636			
637	10	Empirical cumulative distribution of event termination time for the conceptual model with values of $r = 0, 40\%, 60\%$ for $b = 0.24/\text{mon}$, $c = 0.33/\text{mon}$ and $d = 0.26/\text{mon}$ (region 1)	39
638			
639			

- 640 11 Mean termination time (in month) for cold events minus that for warm events
641 in the conceptual model, with $r = 60\%$ and $b = 0.24/\text{mon}$. The thick lines
642 separate regions of different stability as in Figure 3. Grey line is the zero
643 skewness contour from Figure 9. Star markers refer to sample temperature
644 anomaly time series in Figure 4. 40
- 645 12 Termination time for (a) warm and (b) cold events averaged across region
646 2, as a function of stochastic forcing amplitude with $r = 0.6$. Solid line
647 represents the mean. Dashed lines represent the 95-th and 5-th percentiles of
648 the termination time. 41
- 649 13 Conditional probability of warm-to-cold transition minus that of cold-to-warm
650 transitions, for $r = 60\%$, across the c - d parameter space. 42
- 651 14 Changes in transition probabilities with increasing stochastic forcing intensity
652 and fixed $r = 60\%$ for region 2 (self-sustained oscillations). Results are aver-
653 aged within the region that have $\text{Probability}(\text{Warm-to-cold}) = \text{Probability}(\text{Cold-}$
654 $\text{to-warm}) = 1$ when stochastic forcing is absent. 43
- 655 15 Regions in the parameter space where the skewness (magenta, solid lines),
656 warm-to-cold transition probability minus cold-to-warm transition probabil-
657 ity (cyan, dotted line) and differences in termination time (yellow, dashed
658 lines) are closest to the required values given by observations ($r=20\%$), CM2.1
659 ($r=40\%$) and CM2.5 ($r=20\%$); see Table 2. Lighter regions correspond to er-
660 rors less than 50% of the targeted statistics. Darker regions correspond to
661 errors less than 15%. 44

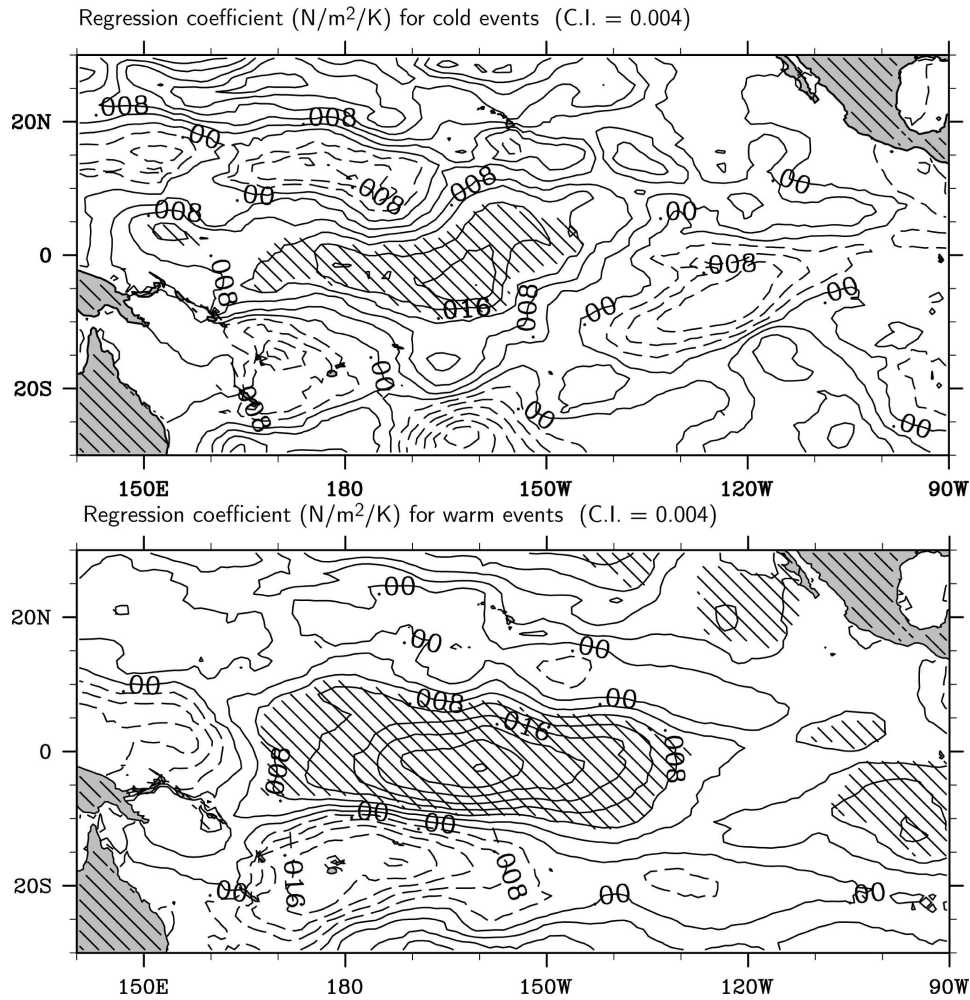


FIG. 1. Regression coefficient of FSU zonal wind stress anomalies onto the HadISST Niño-3.4 index, for Niño-3.4 greater than 0.5K (top) and less than -0.5K (bottom). Regions with confidence level exceeding 60% are hatched.

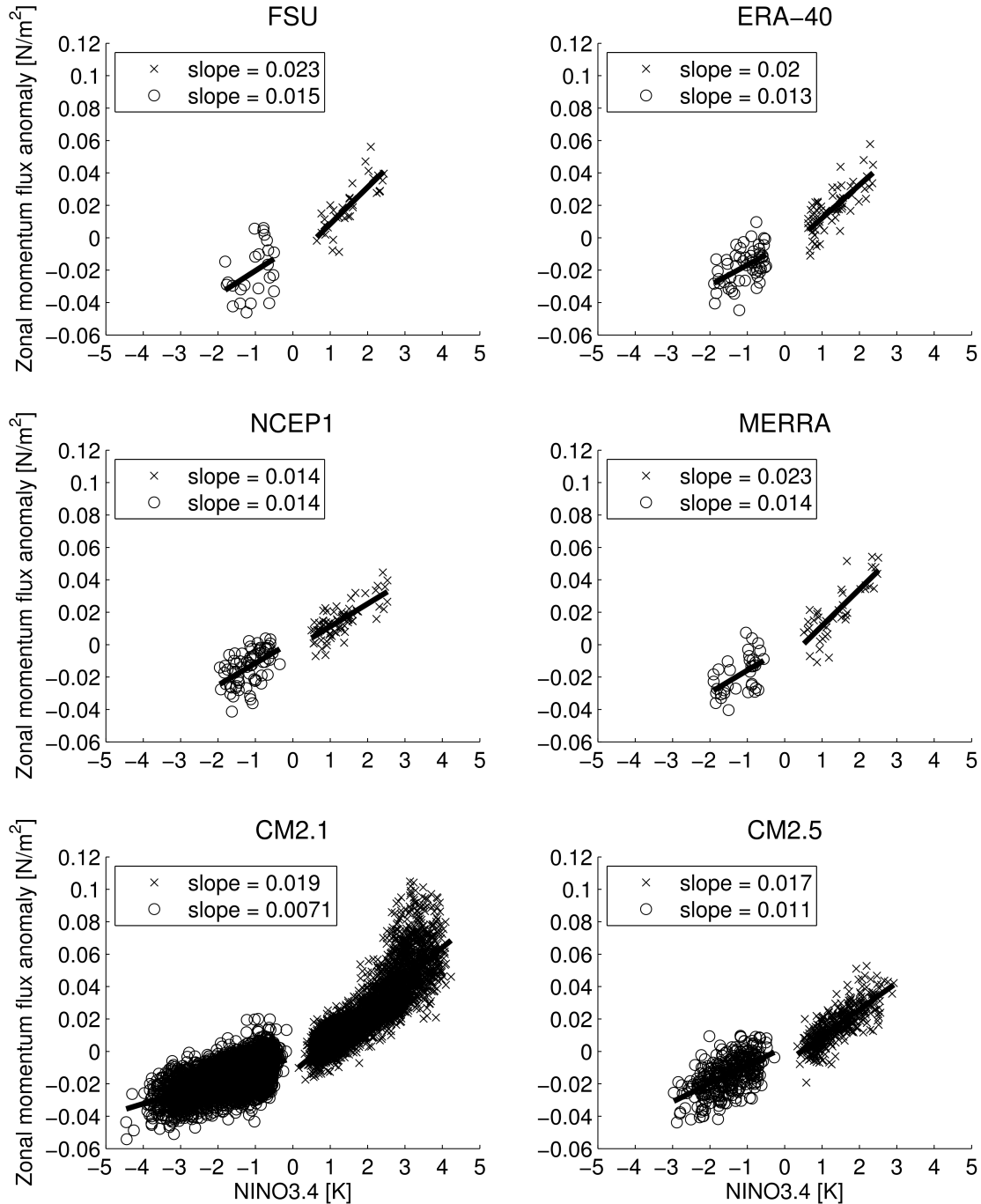


FIG. 2. Regression coefficient of the area averaged zonal wind stress anomalies onto the Niño-3.4 index, for Niño-3.4 greater than 0.5K (top) or less than -0.5K (bottom). The HadISST Niño-3.4 index is used for the FSU and ERA-40 regression analysis. Reanalysis wind stress anomalies are regressed onto the reanalysis Niño-3.4 indices, for MERRA and NCEP-1 respectively. Model wind stress anomalies are regressed onto the model Niño-3.4 index. Area averages of the wind stress are computed within the 40-degree longitude box spanning from 5°S to 5°N where the regression coefficient is the largest across the equatorial Pacific domain. For warm events, wind stress anomalies are averaged within a box sits at 177W-137W (FSU), 176E-144W (ERA-40), 176W-136W (NCEP-R1), 179W-139W (MERRA), 167E-153W (CM2.1), 170E-150W (CM2.5). For cold events, the box sits at 171E-149W (FSU), 153E-167W (ERA-40), 160E-160W (NCEP-R1), 167E-153W (MERRA), 140E-180E (CM2.1), 140E-180E (CM2.5).

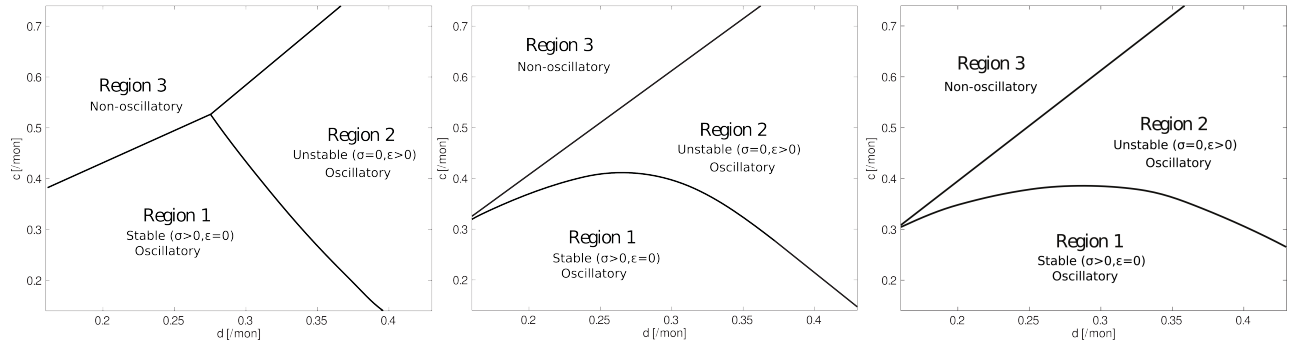


FIG. 3. Stability characteristics of the conceptual model in the c - d parameter space, with $b = 0.24/\text{mon}$ and $r = 0$ (left), $r = 20\%$ (middle), $r = 60\%$ (right), Region 1: the system is linearly stable and sustained by normally distributed stochastic forcing ($\sigma > 0, \epsilon = 0$). Region 2: the system is linearly unstable but is limited by additional damping ($\epsilon > 0$); there is no stochastic forcing ($\sigma = 0$). Region 3: unstable, non-oscillatory and is not considered in the current study.

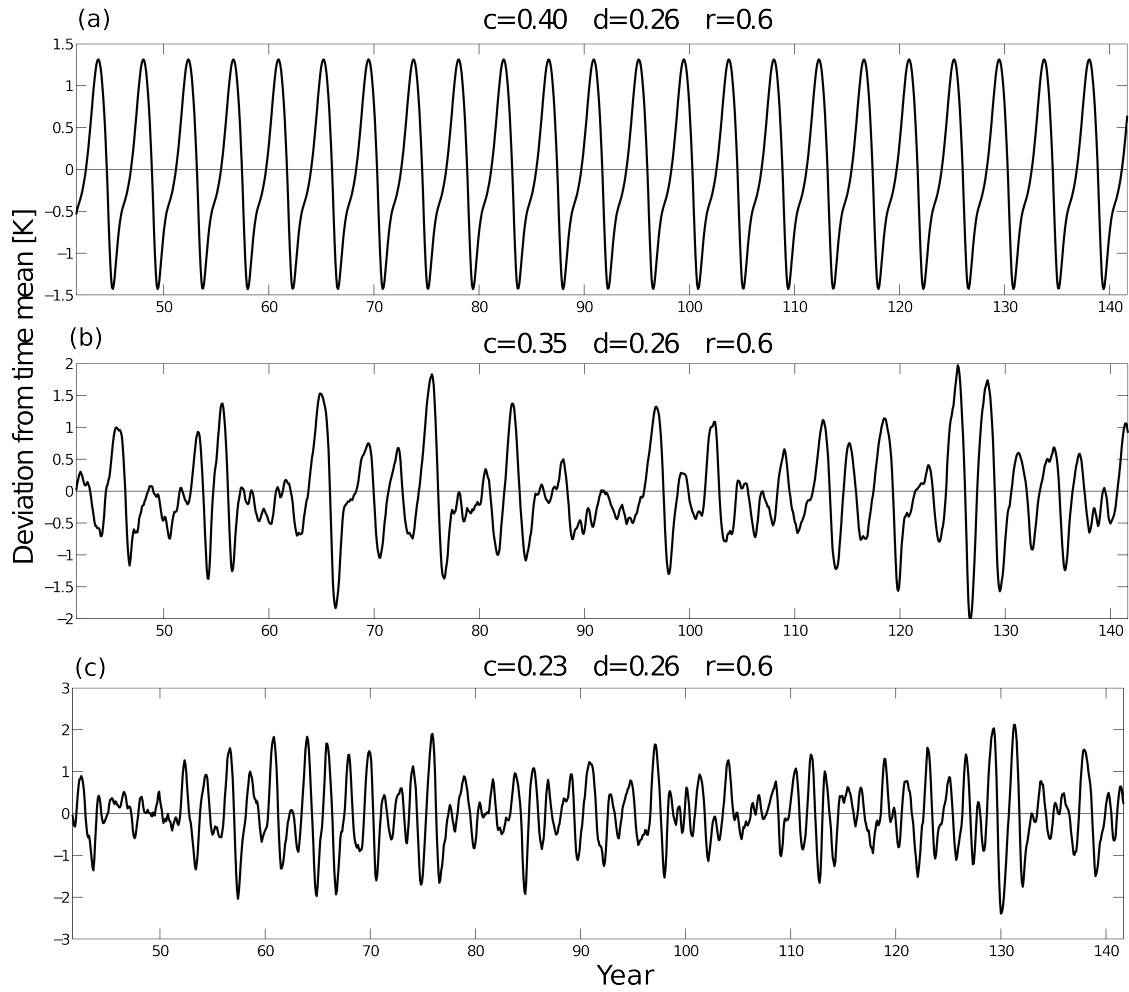


FIG. 4. Sample time series of temperature anomalies. Locations in the parameter space are shown in Figure 11. (a) is an example of self-sustained oscillations free of stochastic forcings. (b) and (c) are examples of stochastically driven oscillations in a stable system.

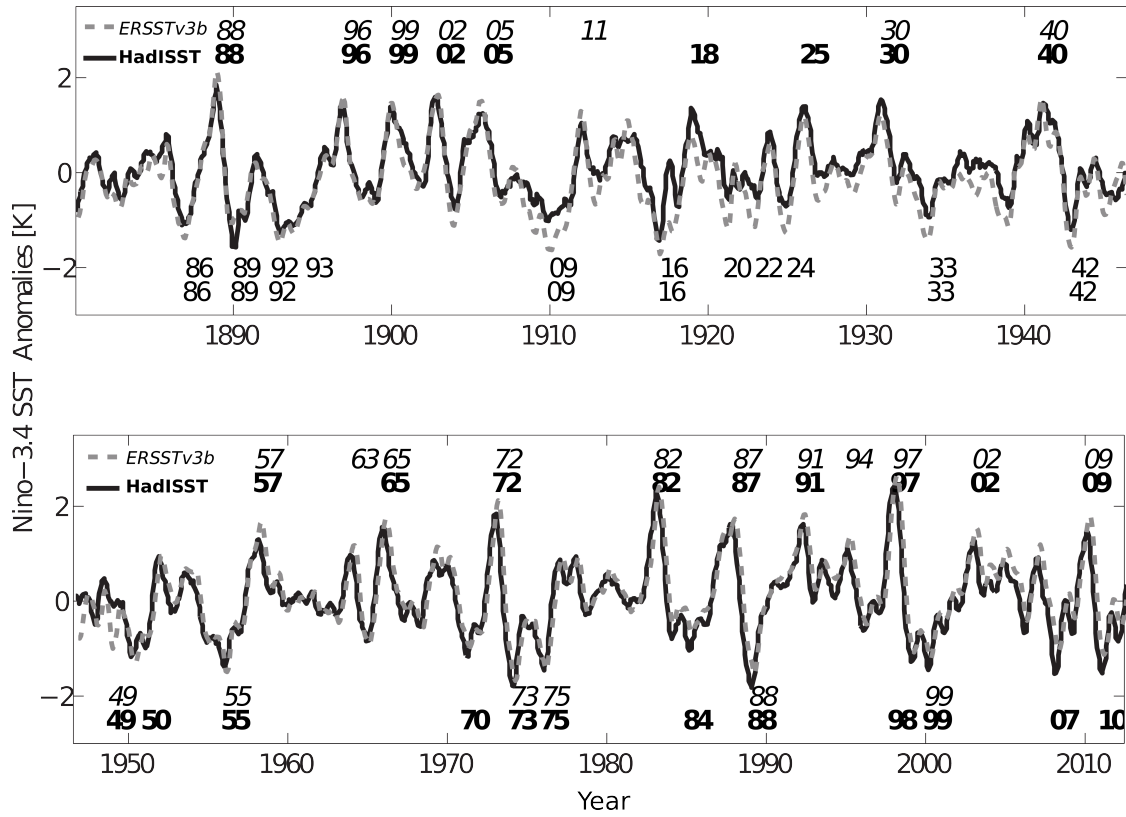


FIG. 5. Winter years of warm and cold events identified using the percentiles criteria on HadISST (solid line) and ERSSTv3b (dashed line) datasets. Numbers above (below) the time series indicate the years when warm (cold) events peak.

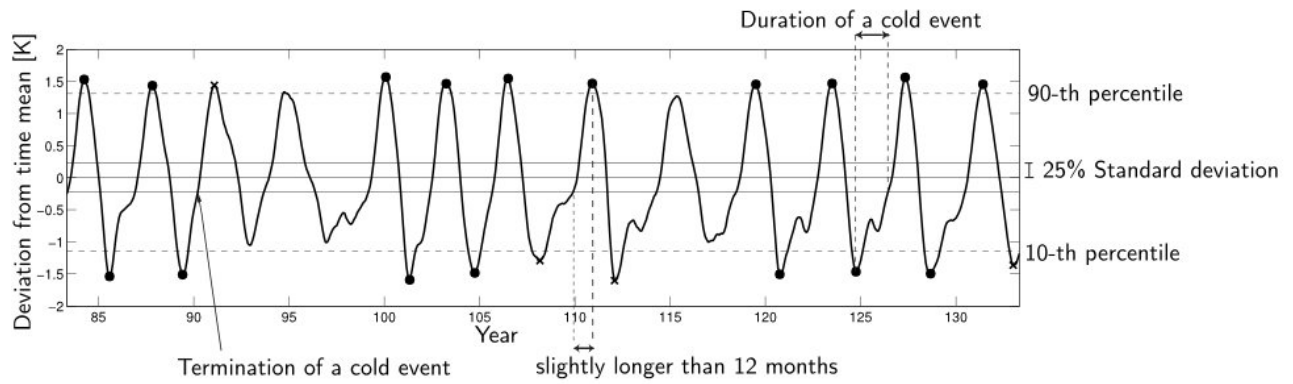


FIG. 6. A sample SST anomaly time series, filtered by 5-month running mean, illustrates how terminations, durations and transitions are defined. The segment is simulated using the conceptual model with $b = 0.24/\text{mon}$, $c = 0.49/\text{mon}$, $d = 0.26/\text{mon}$, $r = 0.6$, $\epsilon = 0.07\text{K}^{-2}\text{mon}^{-1}$ and $\sigma = 0.08\gamma \times 7\text{K} \approx 0.01\text{Nm}^{-2}$ if $\gamma = 0.02\text{Nm}^{-2}/\text{K}$. Filled circles indicate event peaks that are followed by an event of the opposite sign. Crosses indicate event peaks that are not followed by an event, under the criteria described in Section 3.

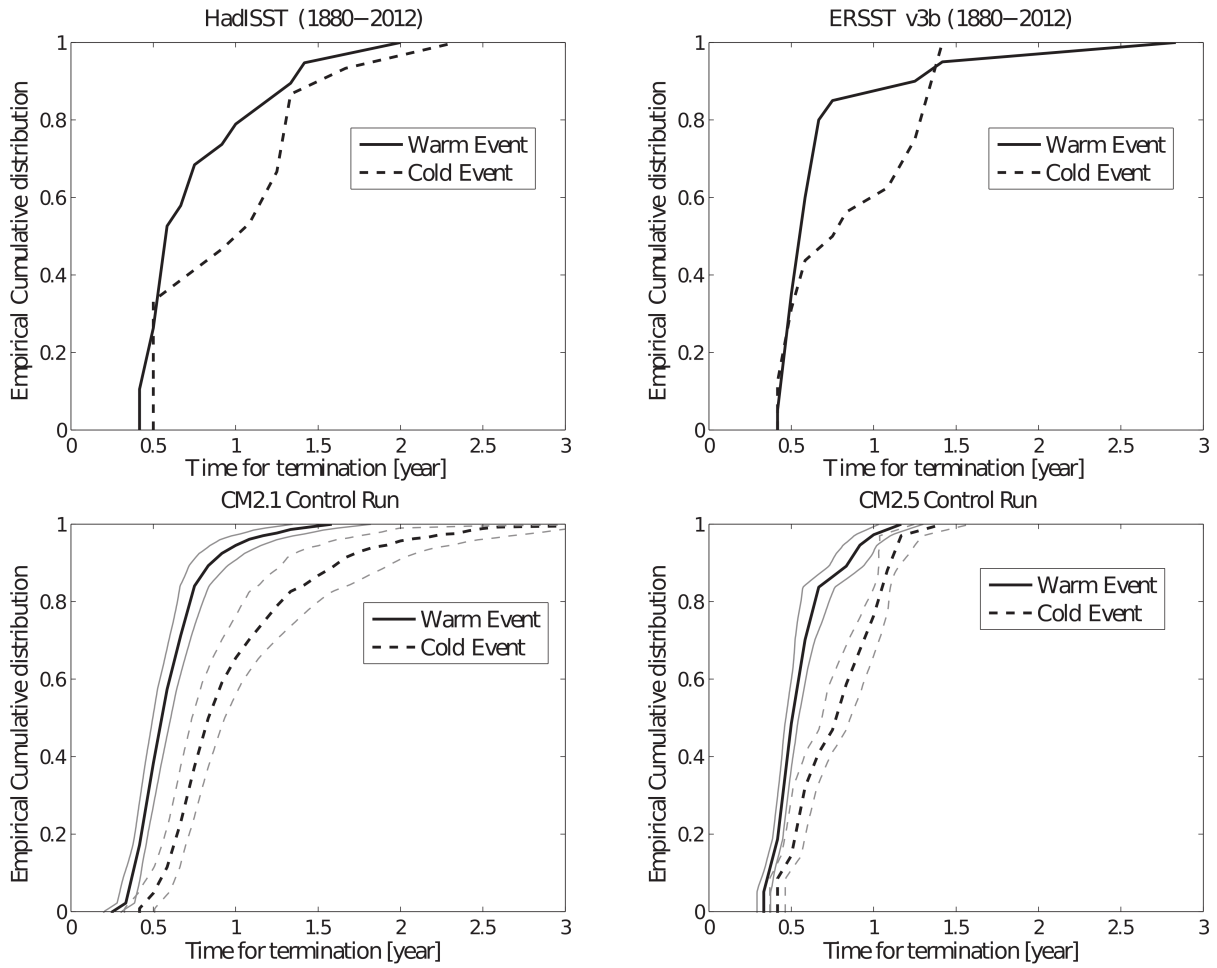


FIG. 7. Empirical cumulative distribution of event termination time using HadISST, ERSST, CM2.1, and CM2.5. The thick lines represent results using the entire time series. For the conceptual models, thin lines represent the standard deviation among 100-year samples.

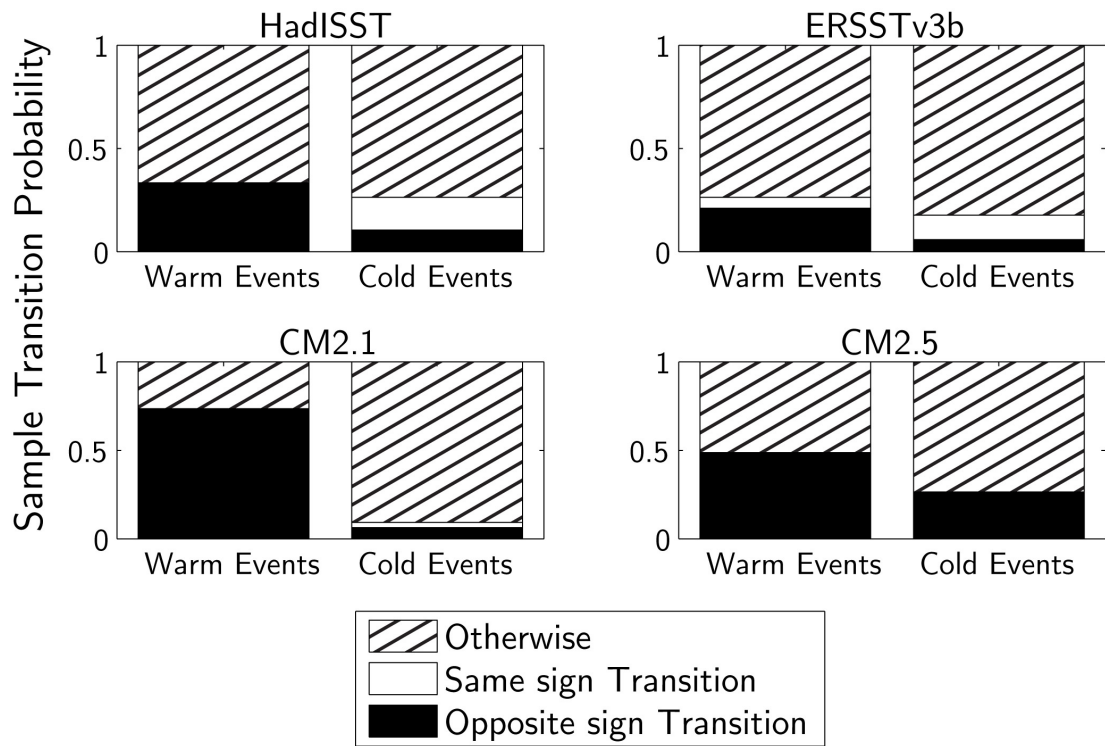


FIG. 8. Conditional Probability of transitions for warm and cold events using Niño-3.4 index

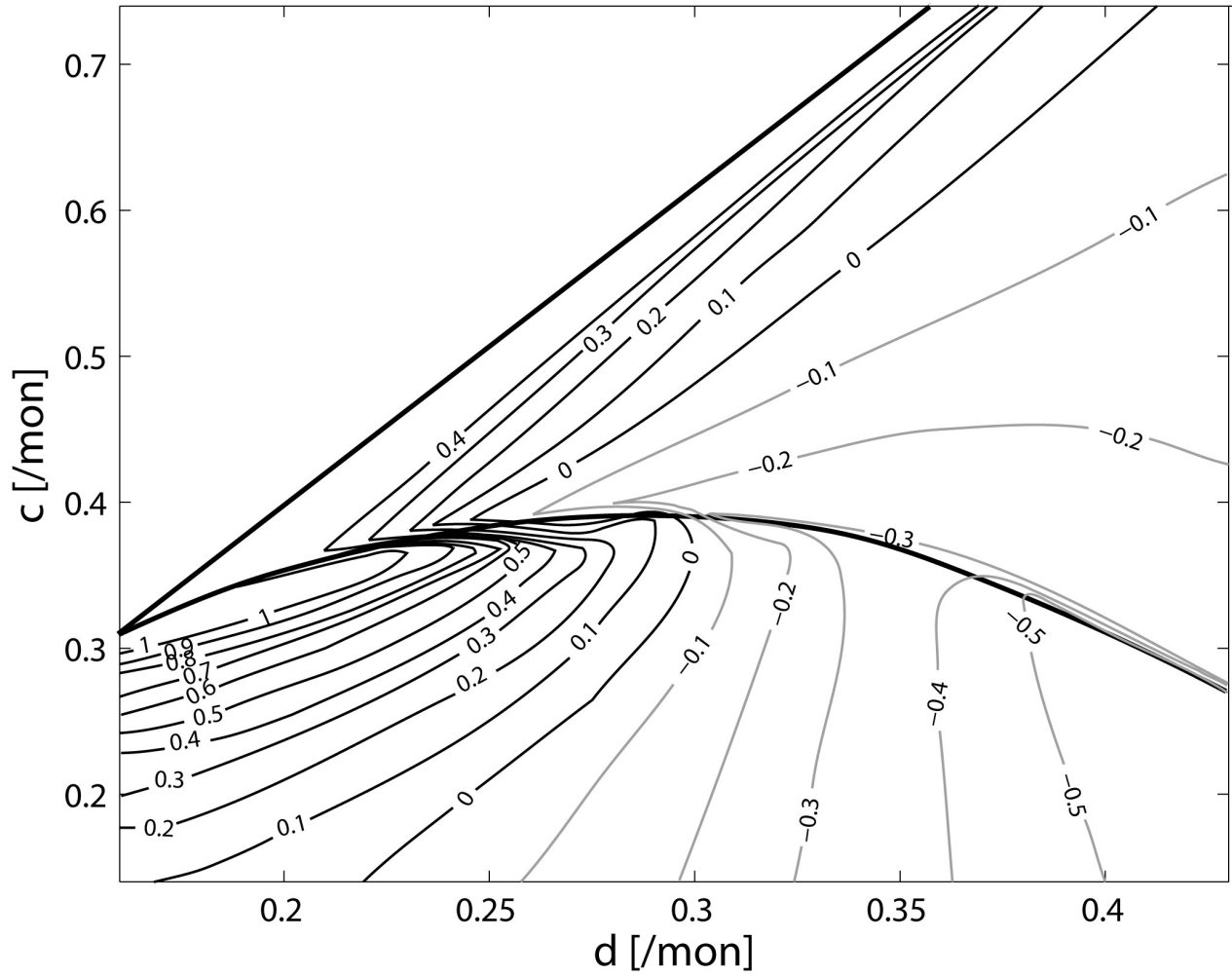


FIG. 9. Skewness of the simulated SST anomalies for the conceptual model with $r = 60\%$

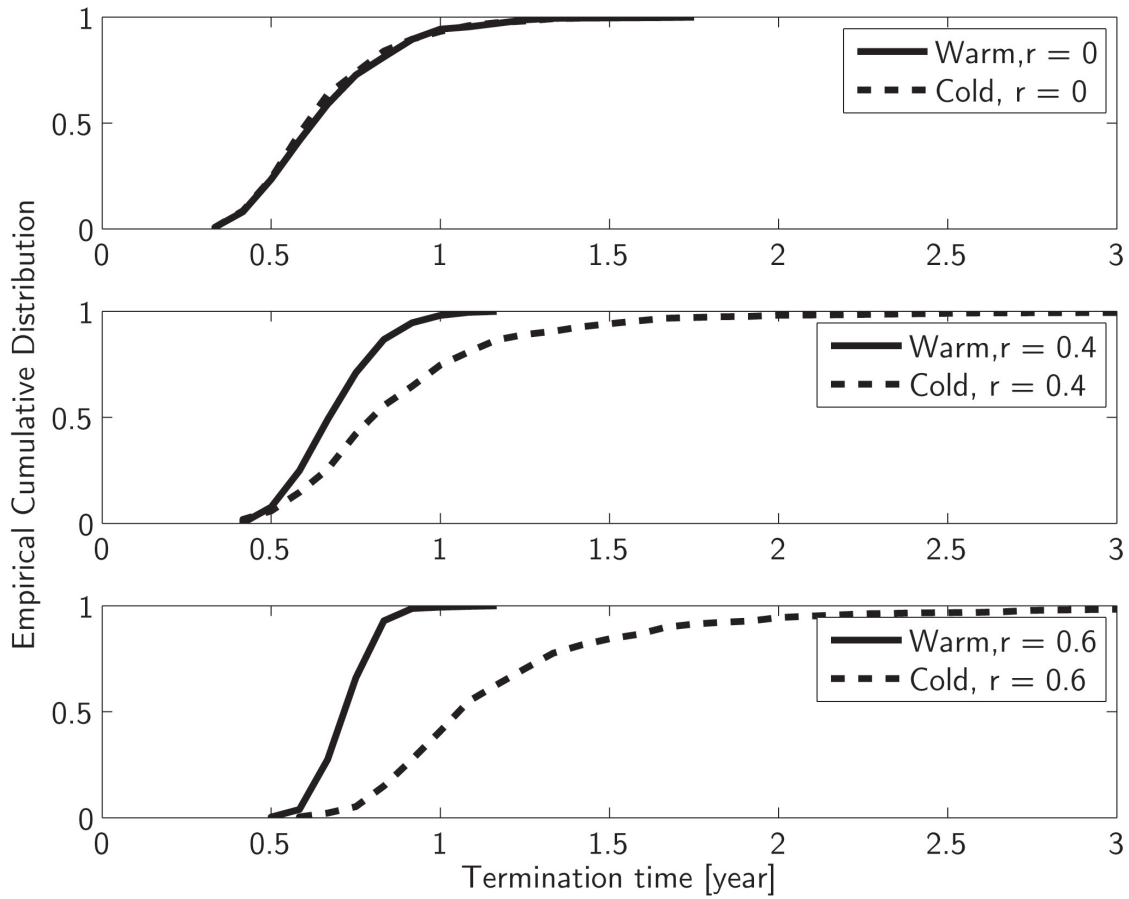


FIG. 10. Empirical cumulative distribution of event termination time for the conceptual model with values of $r = 0, 40\%, 60\%$ for $b = 0.24/\text{mon}$, $c = 0.33/\text{mon}$ and $d = 0.26/\text{mon}$ (region 1)

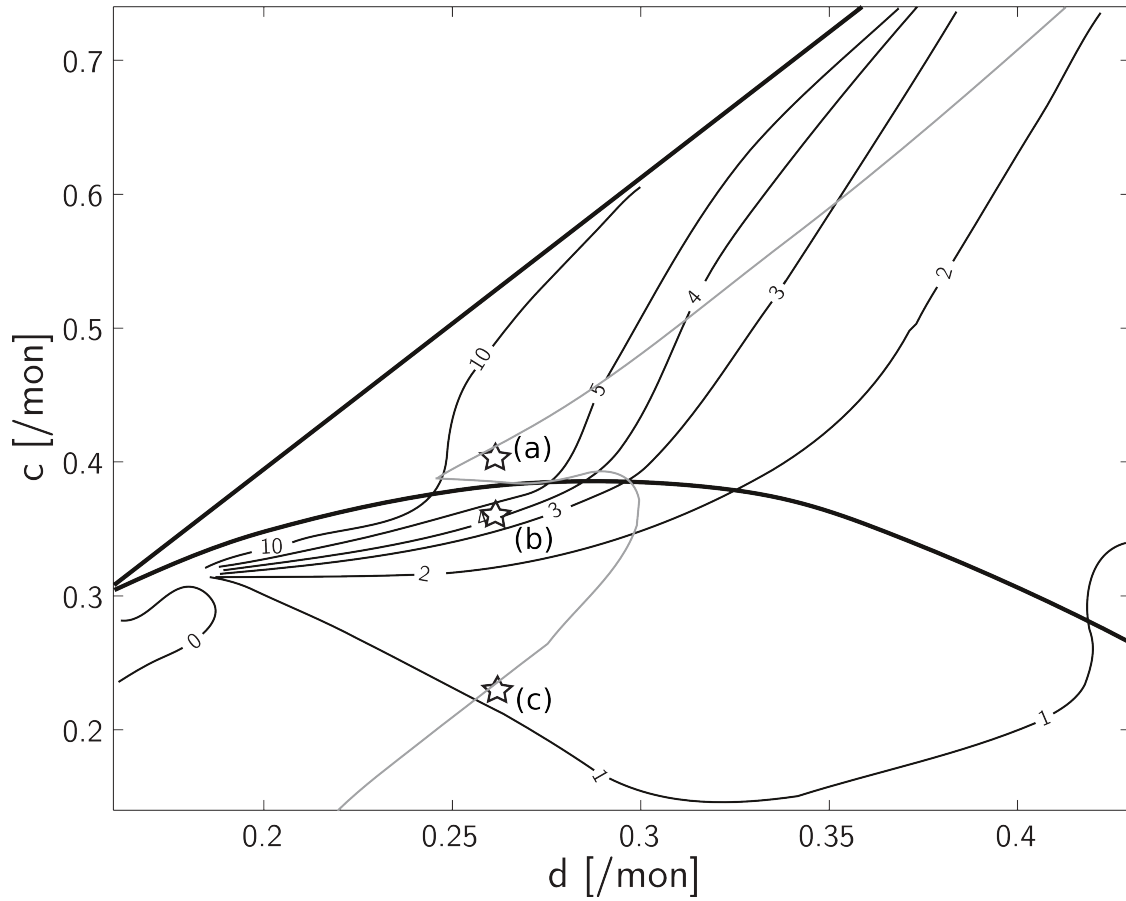


FIG. 11. Mean termination time (in month) for cold events minus that for warm events in the conceptual model, with $r = 60\%$ and $b = 0.24/\text{mon}$. The thick lines separate regions of different stability as in Figure 3. Grey line is the zero skewness contour from Figure 9. Star markers refer to sample temperature anomaly time series in Figure 4.

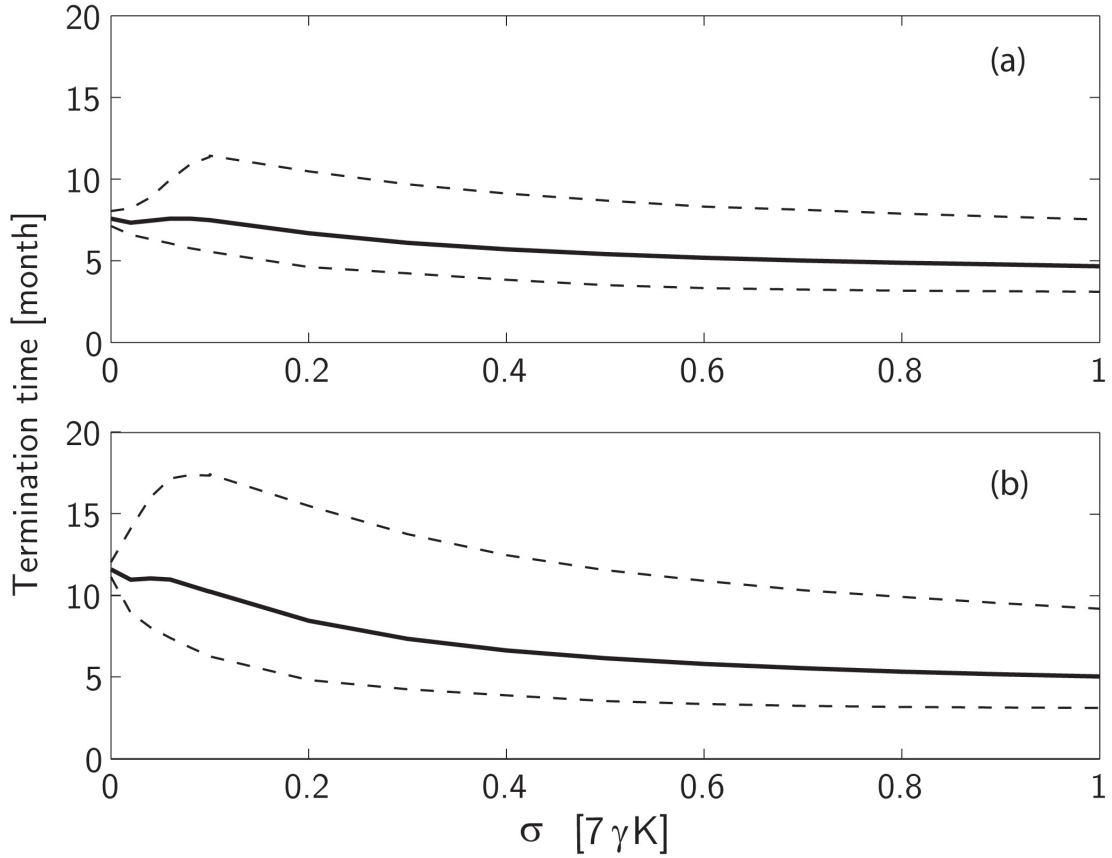


FIG. 12. Termination time for (a) warm and (b) cold events averaged across region 2, as a function of stochastic forcing amplitude with $r = 0.6$. Solid line represents the mean. Dashed lines represent the 95-th and 5-th percentiles of the termination time.

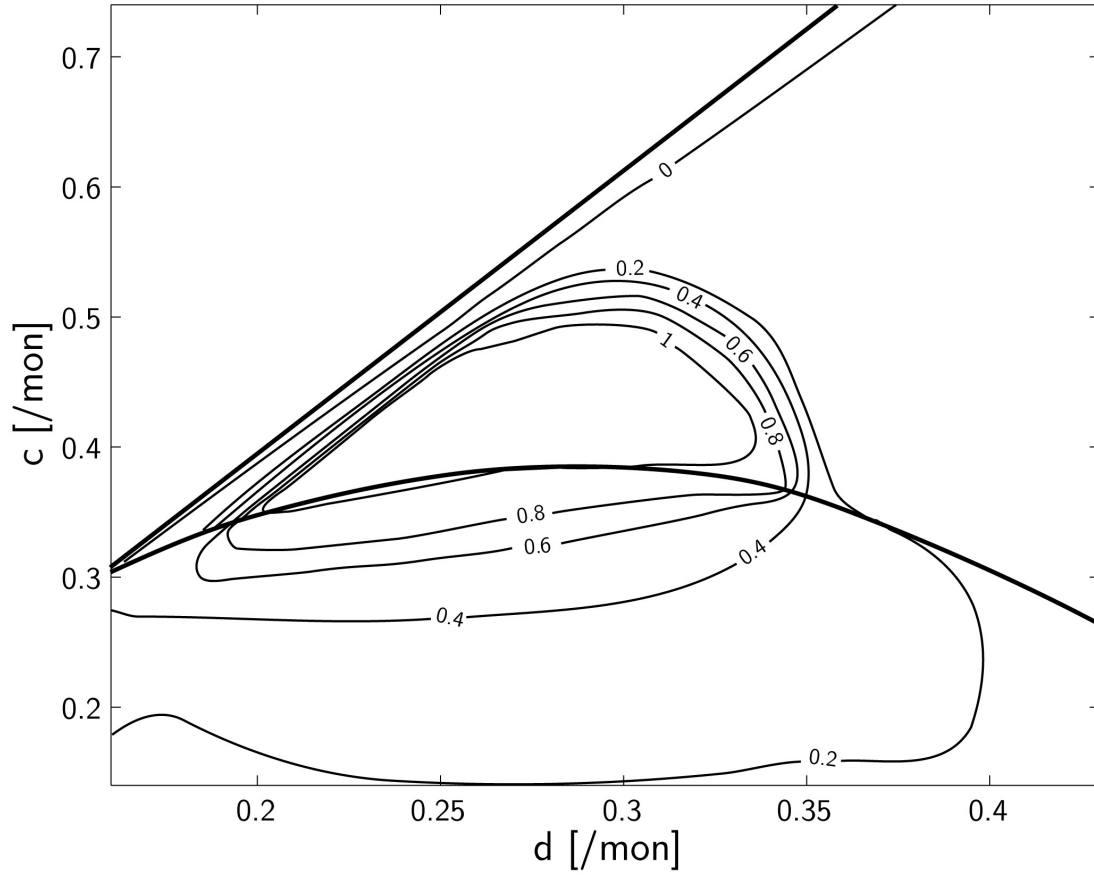


FIG. 13. Conditional probability of warm-to-cold transition minus that of cold-to-warm transitions, for $r = 60\%$, across the c - d parameter space.

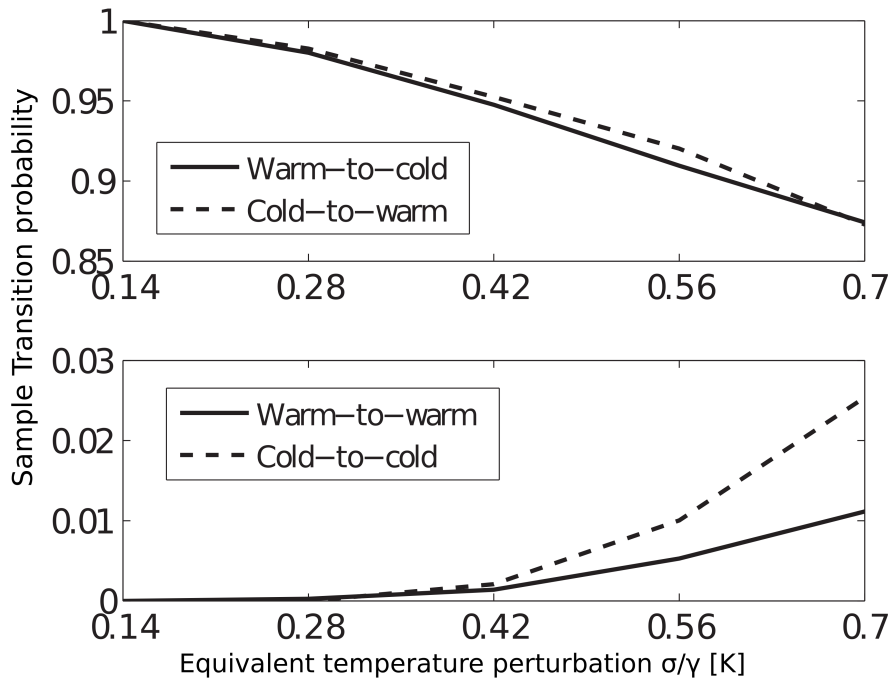


FIG. 14. Changes in transition probabilities with increasing stochastic forcing intensity and fixed $r = 60\%$ for region 2 (self-sustained oscillations). Results are averaged within the region that have $\text{Probability}(\text{Warm-to-cold}) = \text{Probability}(\text{Cold-to-warm}) = 1$ when stochastic forcing is absent.

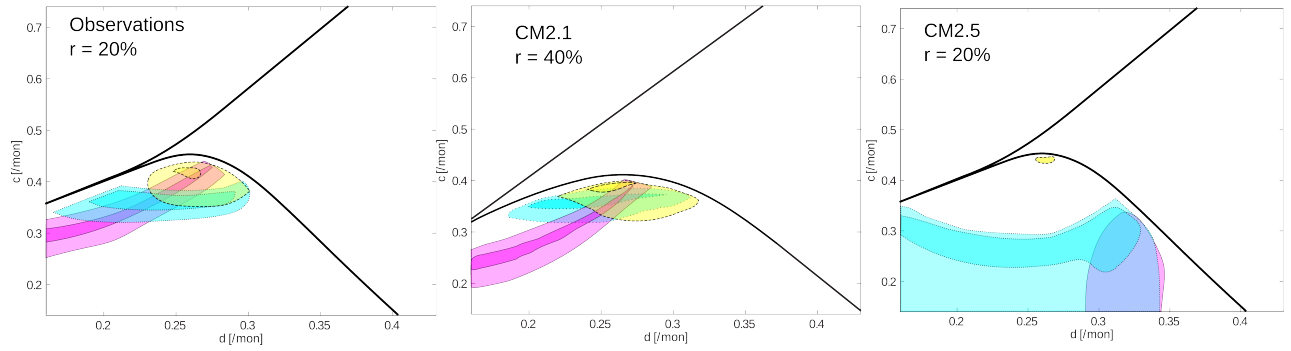


FIG. 15. Regions in the parameter space where the skewness (magenta, solid lines), warm-to-cold transition probability minus cold-to-warm transition probability (cyan, dotted line) and differences in termination time (yellow, dashed lines) are closest to the required values given by observations ($r=20\%$), CM2.1 ($r=40\%$) and CM2.5 ($r=20\%$); see Table 2. Lighter regions correspond to errors less than 50% of the targeted statistics. Darker regions correspond to errors less than 15%.

662 List of Tables

- 663 1 Values of r estimated from linear regression analysis between wind stress
664 anomalies and Niño-3.4 SST anomaly index. The column shows the data
665 sources for the the Niño-3.4 SST anomaly index used in regressions. The row
666 shows the data sources for the zonal wind stress anomalies. 46
- 667 2 Parameters that produce the best simulations of observed, CM2.1 and CM2.5
668 asymmetry statistics. b is fixed at 0.24/month. r are also fixed at values
669 based on the zonal wind stress analysis. Std = Standard deviation of the
670 temperature anomaly (in Kelvin); Skewness= Skewness of the temperature
671 anomaly; LenDiff = Termination time of cold events minus that of warm
672 events (in months); Pdiff = Probability of warm-to-cold transitions minus
673 that of cold-to-warm transitions. The row(s) below Best Fit correspond to the
674 asymmetry statistics derived from the Niño-3.4 SSTA index. Parenthesized
675 values show statistics computed from the first and second halves of the Niño-
676 3.4 SSTA index time series. 47

TABLE 1. Values of r estimated from linear regression analysis between wind stress anomalies and Niño-3.4 SST anomaly index. The column shows the data sources for the the Niño-3.4 SST anomaly index used in regressions. The row shows the data sources for the zonal wind stress anomalies.

	τ_x anomaly dataset				
	ERA-40	ERA-Interim	FSU	MERRA	NCEP
HadISST	0.21	0.12	0.21	0.19	-0.09
NCEP	–	–	–	–	0.00
MERRA	–	–	–	0.24	–
ERA-Interim	–	0.23	–	–	–
ERA40	0.24	–	–	–	–

TABLE 2. Parameters that produce the best simulations of observed, CM2.1 and CM2.5 asymmetry statistics. b is fixed at 0.24/month. r are also fixed at values based on the zonal wind stress analysis. Std = Standard deviation of the temperature anomaly (in Kelvin); Skewness= Skewness of the temperature anomaly; LenDiff = Termination time of cold events minus that of warm events (in months); Pdiff = Probability of warm-to-cold transitions minus that of cold-to-warm transitions. The row(s) below Best Fit correspond to the asymmetry statistics derived from the Niño-3.4 SSTA index. Parenthesized values show statistics computed from the first and second halves of the Niño-3.4 SSTA index time series.

Observations								
	r	Std	Skewness	LenDiff	Pdiff	b	c	d
Best Fit	0.2	0.7	0.26	0.52	0.43	0.24	0.37	0.24
HadISST		0.72 (0.68,0.75)	0.34 (0.26,0.43)	0.9 (-0.4,2.9)	0.15 (0,0.2)			
ERSST		0.77 (0.72,0.79)	0.38 (0.35,0.38)	2.1 (-1.1,4.0)	0.11 (-0.1,0.3)			
CM2.1								
Best Fit	0.4	1.0	0.28	1.9	0.6	0.24	0.36	0.25
Niño3.4		1.2	(0.28,0.34)	(3.3,3.4)	0.6			
CM2.5								
Best Fit	0.2	1.1	-0.13	0.4	0.05	0.24	0.28	0.31
Niño3.4		1.1	(-0.16,-0.06)	(2.2,2.8)	0.11(0.08,0.12)			